Received: 7 December 2022 | Revised: 27 October 2023 | Accepted: 31 October 2023

DOI: 10.1002/joc.8306

RESEARCH ARTICLE

International Journal of Climatology RMetS

Trend analysis of widespread heat days in the Middle East and North Africa region between 1871 and 2012

Mohammad Rezaei[1] | **Mehdi Aalijahan**[2] | **Anthony R. Lupo**[3] | **Hadi Zerafati**[4]

[1]Department of Geography, Tarbiat Modares University, Tehran, Iran

[2]Faculty of Human and Social Sciences, Geography Department, Marmara University, Istanbul, Turkey

[3]Department of Soil, Environmental, and Atmospheric Sciences, University of Missouri, Columbia, Missouri, USA

[4]Department of Physical Geography, Tarbiat Modares University, Tehran, Iran

Correspondence
Mohammad Rezaei, Department of Geography, Tarbiat Modares University, Tehran, Iran.
Email: mohmmad.rezaey@modares.ac.ir

Abstract

One of the greatest challenges facing the world today is global warming. Long-term analysis of spatiotemporal variations in widespread heat days (WHDs) is one approach to monitoring this phenomenon, rather than focusing on the temperature trend. The objective of this study was to reconstruct the temporal and spatial variation of WHDs in the Middle East and North Africa (MENA) using the long-term NOAA/CIRES/DOE 20th Century Reanalysis (V2) (20CRv2) reanalysis data between 1871 and 2012. Based on a 90% probability of occurrence, the temperature threshold for detecting WHDs was defined to be different for each grid point. Then, most WHDs of each month (142 samples) were identified based on the connected component labelling method. The results showed that most WHDs for each month occurred mainly after 2000. In general, the western parts of Iran, Syria, southern Turkey, Saudi Arabia, Kuwait, Egypt and northern Sudan had the highest density of WHDs. In the second period (1941–2012), the extent of WHDs increased compared to the first period (1871–1941). The spatial relationship between WHDs density in the first and second periods showed no statistical relationship, indicating that WHDs were completely different in the two periods. The results of this study contribute to a better understanding of the effects of global warming by using the relatively longest data sets. The comparison between the two periods shows that the WHDs in MENA have changed in extent (instead of variability).

KEYWORDS

MENA region, reconstruction, trend analysis, widespread heat days

1 | INTRODUCTION

The term climate change refers to the change in climate patterns caused mainly by greenhouse gas emissions from natural systems and human activities (Fawzy et al., 2020). Global climate change is one of the major concerns of humanity in the 21st century, and numerous studies have been conducted on its impact on the planet (Konisky et al., 2016; Marx et al., 2021; Ying et al. 2017; Zheng et al., 2019). As one of the aspects of global climate change affected by human activities, global warming is of great concern to humanity (Al-Ghussain, 2019; Varotsos et al. 2019). According to the IPCC reports, human activities have increased the intensity of temperatures and more than doubled the probability of heat waves in some places (IPCC, 2023; Zittis et al., 2016).

It is estimated that the Earth's temperature has increased by 0.08°C per decade since 1880, but more than doubled to 0.18°C per decade since 1981 (Lindsey & Dahlman, 2020). Global warming has caused significant

damage throughout the world in recent decades. Consequences of global warming include droughts (Trenberth et al., 2014), heavy rainfall (Yadollahie, 2019), increased insect populations (Robinet & Roques, 2010), forest fires (Peters, 1990), a decline in fish populations (Lehtonen, 1996) and human health problems (McMichael et al., 2006).

Extreme high temperatures can damage agricultural production, increase energy and water consumption and have negative effects on the ecosystems, health, water resources and evapotranspiration rates (Campbell et al., 2018; Easterling et al., 2000; Karl & Easterling, 1999; Kunkel et al., 1999; Middleton & Sternberg, 2013; Miller et al., 2008). Many studies have shown a general increase in hot days and the decrease in cold days (Robeson, 2004). Heat waves, which are extreme weather events, can have a significant impact on human health, agriculture and energy systems (Thomas et al., 2020). Therefore, heat waves can be employed as an indicator to investigate extreme temperatures. The high-temperature days where the temperature exceeds standard values are identified as heat waves (Ding et al., 2010). In drylands, extreme high temperatures exacerbate potentially stressed human and biophysical conditions (Cueto et al., 2010). For example, during July 1995, a heat wave caused 525 deaths in Chicago (Changnon et al., 1996). Additionally, during the summer of 2003 in France, there were about 15,000 heat-related deaths (Koppe et al., 2004).

Due to drought and water crisis, the Middle East is one of the regions most affected by global warming (Alahmad et al., 2020; Bou-Zeid & El-Fadel, 2002; Kostopoulou et al., 2014). The impacts of climate change will be severe throughout the Middle East and North Africa (MENA), where the climate is hot and dry (Ahmadalipour & Moradkhani, 2018). Natural disasters, droughts, water scarcity, population, income and climate changes may affect the Middle East region with its semi-arid climate (Hameed et al., 2020). Accordingly, several studies have been conducted in the Middle East on global warming and temperature trend. Several studies have shown that temperatures and heat waves in the Middle East have tended to increase over the past 60 years (Kostopoulou et al., 2014; Perkins-Kirkpatrick & Lewis, 2020; Zhang et al., 2005; Zittis et al., 2016). Some studies have also been conducted at the national level, for example, Kousari et al. (2013) in Iran; Almazroui et al. (2014) in Saudi Arabia; Cheng et al. (2017) in Qatar; Salman et al. (2017) in Iraq; El Kenawy et al. (2019) in Egypt, confirming that temperature has increased since 1960.

However, this increasing trend may be due to natural climate variability, and this variability is an obstacle to reliable determination of global change (Ghil, 2002). Therefore, long-term data can increase the certainty of the study. Recently, several studies have been conducted to reconstruct 20th century climate events around the world using National Oceanic and Atmospheric Administration (NOAA)/Cooperative Institute for Research in Environmental Science (CIRES)/ Department Of Energy (DOE) 20th Century Reanalysis (V2) (20CRv2) data. Compo et al. (2013) used the 20th century reanalysis system to study global warming, ignoring all air temperature observations. According to their results, global warming was confirmed by these data. Aalijahan et al. (2019) studied the temporal–spatial patterns of cold waves below −15°C and their magnitude over 142 years (1871–2012) over northwestern Iran. The results show a reliable correlation between reanalysed data and station data. According to Yang et al. (2021), the 20CRv2 data show better warming trends than other reanalysed data and are very close to observations. Zerafati et al. (2021) studied the temporal changes in temperatures in the West Asian region from 1836 to 2020 using 20CRv2 data. However, they focused on temperatures above 50°C. Therefore, despite the importance of temperature studies, no comprehensive study has been conducted to assess the extent of hot days in the Middle East region using reanalysed 20th century data.

The purpose of this study is to reconstruct the extent of hot days and examine their long-term changes. The results are divided into five sections. In the first section, we examine the long-term trend in temperature. In the second section, heat days are determined based on a threshold. In the next step, extended heat days were determined for each month. In the next section, extended heat days were determined using ERA5 reanalysis data and compared to 20CRv2. In the last section, we examined the long-term trend of extended heat days.

2 | DATA AND METHODOLOGY

2.1 | Study area

The study area is located in the arid and warm belt of the Northern Hemisphere (Gherboudj et al., 2017; Peale, 1966; Rezazadeh et al., 2013), which makes it an attractive area for studying the extent of heat days. The studied area ranges from 0 to 80.5° E and 0 to 44.5° N, as shown in Figure 1. The 20CRv2 reanalysis data have a spatial resolution of 1.87 × 1.9°, so the selected region is covered by 774 pixels.

2.2 | Data and methods

This research reconstructed the widespread heat days (WHDs) in the Middle East using 2-m air temperatures from the NOAA/CooperativeCIRES/DOE 20CRv2 (Slivinski et al., 2019). Long-term climate datasets are critical both for understanding climate variability and for evaluating its simulation in climate models, and the output of these

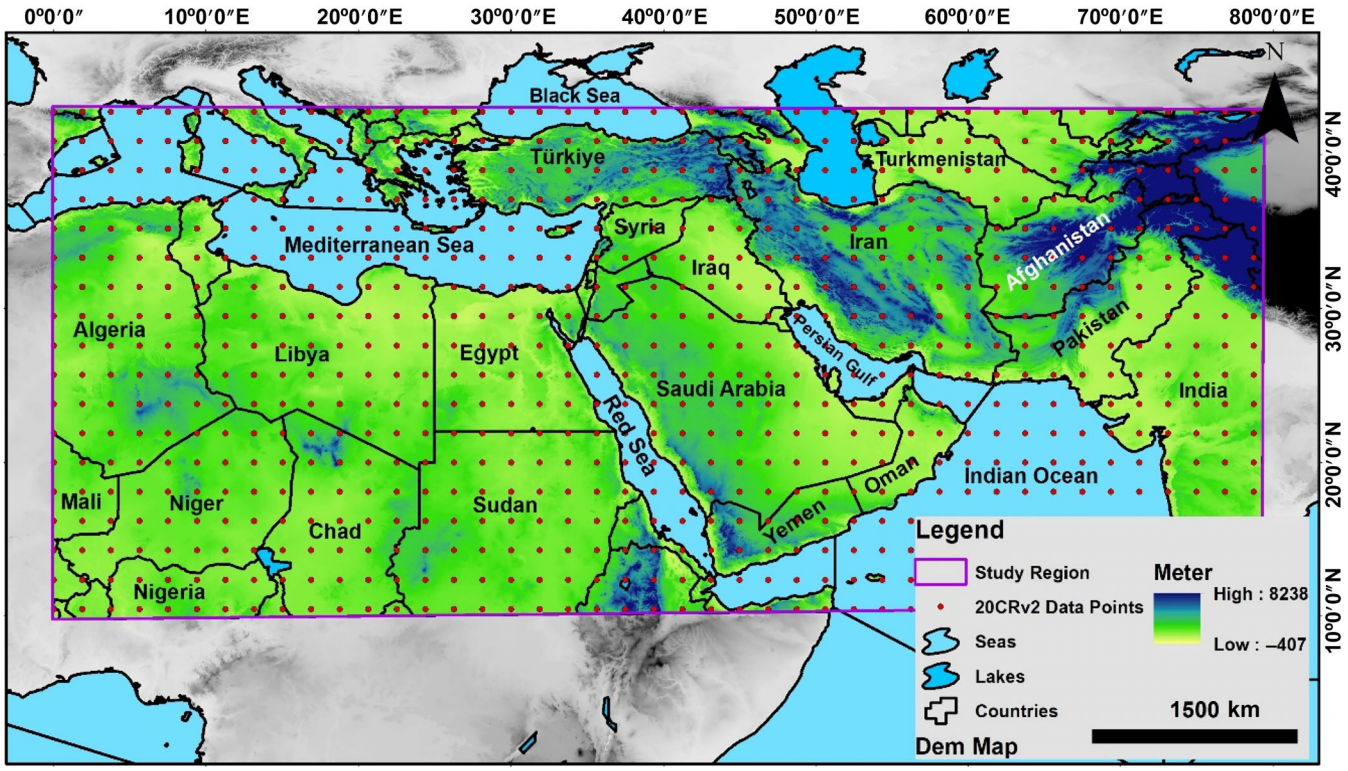

FIGURE 1 The study area for reconstruction of widespread heat days along with 1.87 × 1.9-degree grid points based on the 20CRv2 dataset. [Colour figure can be viewed at wileyonlinelibrary.com]

models is used to assimilate data to generate the 20CRv2 reanalysis datasets. The 20CRv2 dataset provides the first estimates of global tropospheric variability (Compo et al., 2011). We use the updated version of the 20CRv2 data which covers 142 years from 1 January 1871 to 31 December 2012. While the data were produced on a T62 spectral grid with 28 vertical levels, we use the output data on a regular latitude–longitude grid with a cell size of 2° at the near-surface pressure level (about 2 m height). Comparisons with independent radiosonde data show that the reanalyses are generally of high quality. The quality in the extratropical Northern Hemisphere throughout the century is comparable to that of current 3-day operational NWP forecasts. Comparisons of these surface-based reanalysis with other reanalyses that also use upper-air and satellite data are also encouraging (Compo et al., 2011). A full description of the 20CRv2 project can be found in Compo et al. (2011). We used the European Center for Medium-Range Weather Forecasts (ECMWF) Reanalysis v5 (ERA5) (Hersbach et al., 2020) as reference data for comparing 20CRv2 estimates of WHDs.

2.3 | WHDs identification

For the identification of heat days, the numerical threshold for determining a heat day was first established based on the top 10% of the temperature of each point in the period of 142 years (1871–2012). This value may be different for each location based on its climate. Based on this threshold, which was calculated separately for each month and point, the lower values were then removed, and a daily temperature map was drawn. As an example, Figure 2 shows the pixels whose temperature is above the threshold for 31 July 2012. On this day, 26.5% of the pixels in this region were found to have a heat day.

In the next step, the 'connected component labelling method' in the igraph package of R (developed by Csardi, 2013) was applied to the daily heat day map. The method identified nine separate connected heat pixels, the largest of which is shown in Figure 3. This widespread heat covered 20% of the study area and is known as the largest heat day in July 2012. After identifying the most extensive heat days for each month (142 days in the studied period), their spatial and temporal characteristics were analysed.

2.4 | Mann–Kendall test and Sen's slope estimator—trend detection

A nonparametric Mann–Kendall test was used to determine the trend. The nonparametric Mann–Kendall test is widely used in detecting trends of variables in meteorology

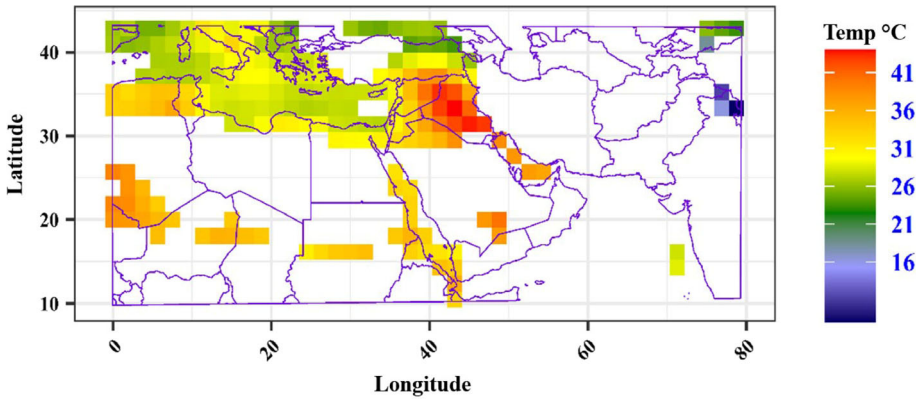

FIGURE 2 Heat pixel for 31 July 2012 (as an example for widespread heat days). [Colour figure can be viewed at wileyonlinelibrary.com]

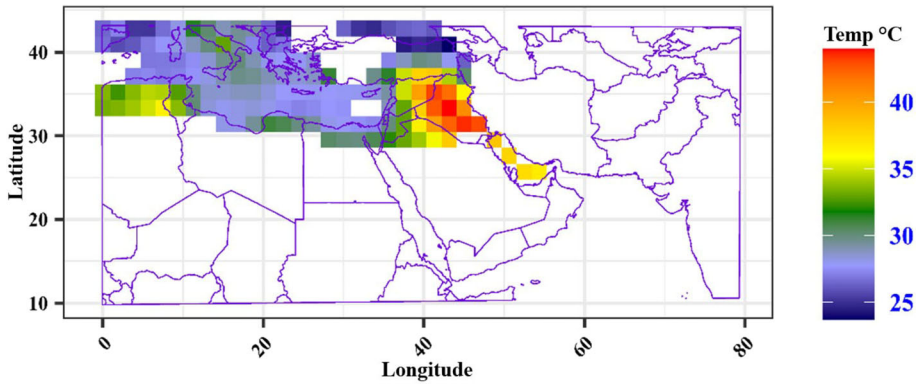

FIGURE 3 The widespread contiguous heat pixel in the previous figure as a selected sample from July 2012. [Colour figure can be viewed at wileyonlinelibrary.com]

and hydrology fields (Aalijahan et al., 2021, 2023; Ahn & Merwade, 2014; Esfandiari & Rezaei, 2022; Liang et al., 2010; Rezaei et al., 2022; Wang et al., 2019) Statistic s can be obtained by Equation (1).

$$s=\sum_{k=1}^{n-1}\sum_{j=k+1}^{n}\operatorname{sgn}\left(x_j-x_k\right), \tag{1}$$

where n is the length of the sample, x_k and x_j are from $k = 1, 2, ..., n-1$ and $j = k+1, ..., n$. If n is bigger than 8, statistic s approximates to normal distribution. The mean of s is 0 and the variance of s can be acquired as follows:

$$\operatorname{var}(s)=\frac{n(n-1)(2n+5)}{18}. \tag{2}$$

Then, the test statistic z is denoted by Equation (3).

$$z\begin{cases}\dfrac{s-1}{\sqrt{\operatorname{var}(s)}}, & \text{if } s>0\\ 0, & \text{if } s>0\\ \dfrac{s+1}{\sqrt{\operatorname{var}(s)}}, & \text{if } s<0\end{cases}. \tag{3}$$

If $z>0$, it indicates an increasing trend, and vice versa. Given a confidence level α, the sequential data would be supposed to experience statistically significant trend if $|z| > z(1-\alpha/2)$, where $z(1-\alpha/2)$ is the corresponding value of $p=\alpha/2$ following the standard normal distribution. In this study, 0.05 and 0.01 confidence levels were used. Besides, the magnitude of a time series trend was evaluated by a simple nonparametric procedure developed by Sen (1968). The trend is calculated by:

$$\beta=\operatorname{median}\left(\frac{x_j-x_i}{j-i}\right), j>i, \tag{4}$$

where β is Sen's slope estimate. $\beta>0$ indicates upward trend in a time series. Otherwise, the data series presents a downward trend during the time period. Figure 4 shows the process of identifying WHDs and analysing their trends in study area.

3 | RESULTS AND DISCUSSION

3.1 | Long-term trends of temperature

Mann–Kendall tests were used to calculate the long-term trend in the frequency of temperature for each month. From 1871 to 2012, the points that showed a significant trend (decrease or increase) were first identified, and then the slope values for each point were calculated.

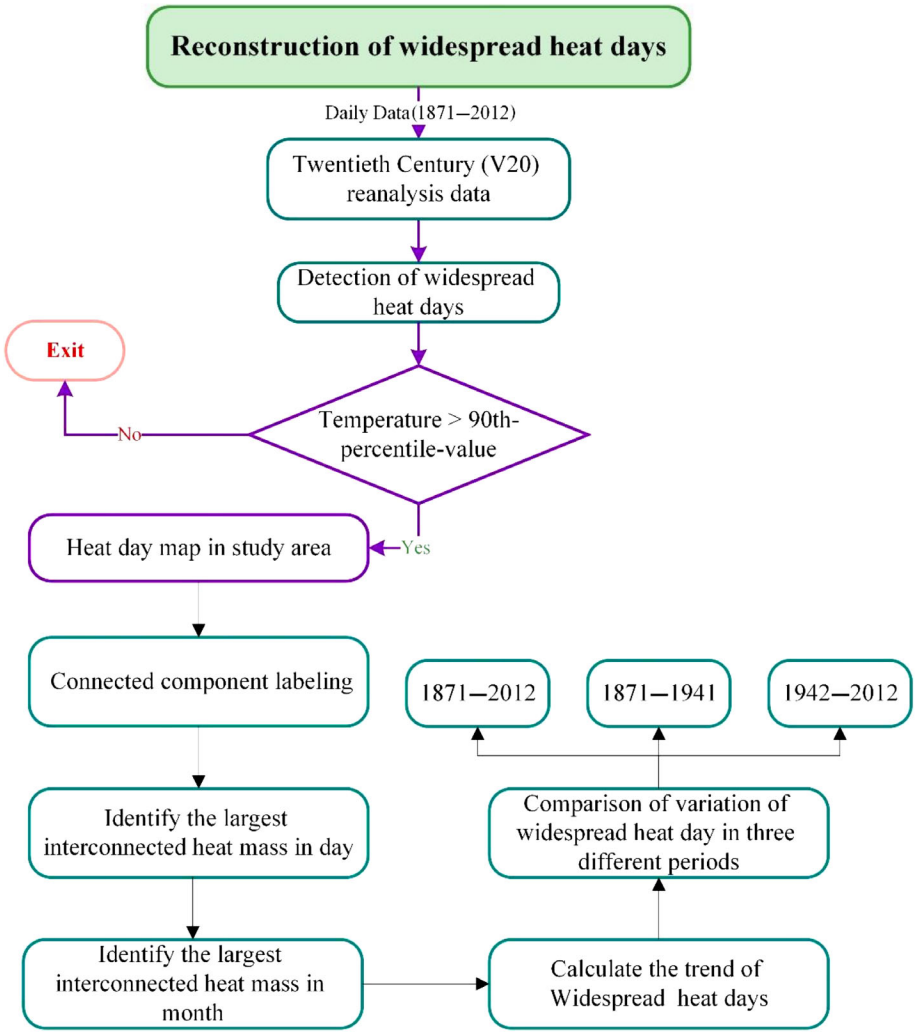

FIGURE 4 The process of reconstructing widespread heat days in the Middle East using 20CRv2 data. [Colour figure can be viewed at wileyonlinelibrary.com]

Figure 5 shows the slope values of the temperature trend from 1871 to 2012. The results show that temperatures increase from August to February in a large part of the studied area. In the central part of the studied region, which includes large parts of the northwest and west of Iran, Turkey, Syria, Iraq and large parts of northeast Africa, the temperature situation changes and adopts a decreasing trend from March to July. Among the months of the year, March shows the largest decrease in temperature with 27%, followed by July with 15%. In January, it reaches its lowest value of 0.002%. Therefore, the largest areas with an increase in temperature are found first in August and then in November, with 64% and 61% of the total study area, respectively. The month of March shows the least tendency of increase in temperature, with 23% of the studied area. Based on the spatial average of Sen's slope, it can be said that the highest and lowest positive of temperature trends are found in November and February, with $0.012_{^\circ C year^{-1}}$ and $0.007_{^\circ C year^{-1}}$ percent, respectively.

Spatially, the lowest (highest) Sen's slope value is observed in July at 35.5° E and 39° N in the central and eastern regions of Turkey (at 76.9° E and 29.5° N in northern India) with a value of $-0.023_{^\circ C year^{-1}}$ ($0.046_{^\circ C year^{-1}}$). The obtained results are consistent with the results of long-term analysis of temperature trends in Turkey and India. As studies show, the temperature trend in Turkey has always increased in the long term, but the eastern regions of Turkey had a slower increase than other regions (Can & Atimtay, 2002; Hadi & Tombul, 2018). In addition, studies in India have shown that the temperature trend in this country has increased in the long term, but maximum temperatures have experienced a stronger upward trend than other temperatures in this region (Amrender et al., 2015; Pal & Al-Tabbaa, 2010). Therefore, it can be seen that the long-term increase in temperature is stronger than its decrease, and the studied area experiences a significant increase in temperature during the 142 years of the study period.

However, dividing the 142 years into two periods, it can be seen that in the first 71-year period from 1871 to 1941, the largest area of regions that showed a decreasing temperature trend was in May and April, with 42% and 35%,

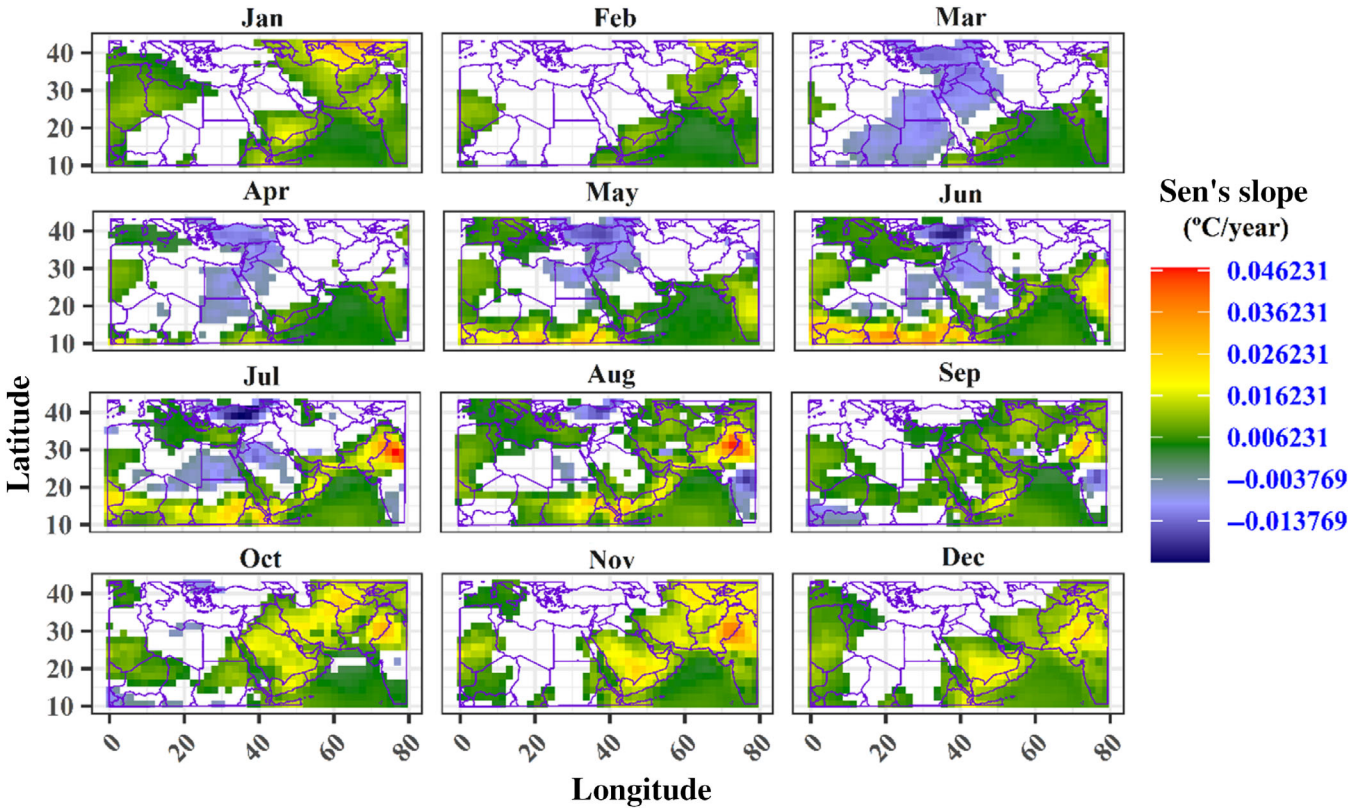

FIGURE 5 Slope values of Sen's determined from the trend of 2-m air temperature in the period from 1871 to 2012. [Colour figure can be viewed at wileyonlinelibrary.com]

respectively. The lowest value, 1%, was observed in February. As for the slope values, the highest negative trend is observed in May with 0.026° per year (Figure 6). As for the geographical region, the lowest Sen's slope (−0.056° per year) is observed in June at the location 5.5° E and 35° N, which is located in the northern regions of Algeria.

February and January have the largest area of increasing temperatures in the first period, with 26% and 24% of the total, respectively. The month of March has the lowest temperature increase with 2% of the studied area. The highest value of positive trend of Sen's slope is observed in the month of February with a rate of 0.025 and the lowest average in the month of October with a rate of 0.007%. The highest Sen's slope in the studied area with a value of 0.058 in February belongs to the point of 65.6° E latitude and 37.1° N, which includes part of the southeast of Tajikistan.

In the second period (1942–2012), the largest percentage of covered area with a decreasing temperature trend is November with 10% and January with 7% (Figure 7). The lowest value occurred in October with an area of 0.01%. For Sen's slope values, the highest negative trend is observed in January and November with −0.025% each. As can be seen in Figure 6, the lowest Sen's slope of −0.036% is observed at points 37.5° E and 39° N in the month of November, almost in the eastern and central Anatolian regions of Turkey. The results of Hadi and Tombul (2018) research also show that a large part of Turkey has experienced a decreasing temperature trend in the autumn season between 1901 and 2014, and most of this decreasing trend is found in the Bingoel region of Eastern Anatolia.

The largest area with increasing temperature trend is first in August and then in September, both with 67% and 62%, respectively, and the smallest proportion is in February and March with 16%. As for Sen's slope, the highest value of positive trend with 0.022 and the lowest value with 0.013% belong to May and January, respectively. The highest value of Sen's slope was reached in May with 0.069%, which is located in the east of Iran at 60° E and 31.4° N. The result of the researchers' study (Mirhoseini et al., 2021) shows that the maximum temperature in Birjand region, which is very close to this region, showed a significant increasing trend in April and May during 1987–2019, which confirms the results of this study.

3.2 | The determination of the heat day

A heat day was determined based on a 90% probability of occurrence (over the 142-year period from 1871 to 2012).

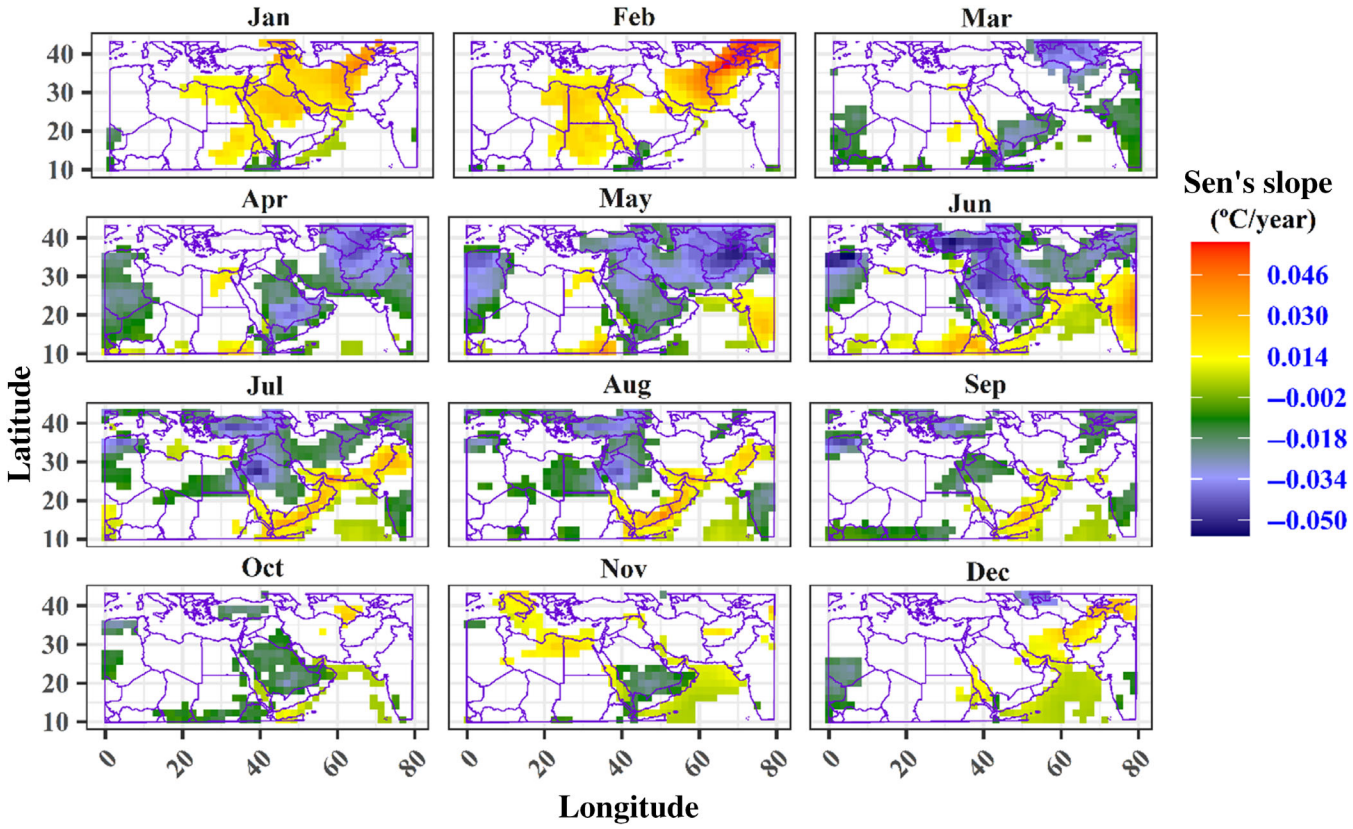

FIGURE 6 Similar to Figure 5, but for the period 1871–1941. [Colour figure can be viewed at wileyonlinelibrary.com]

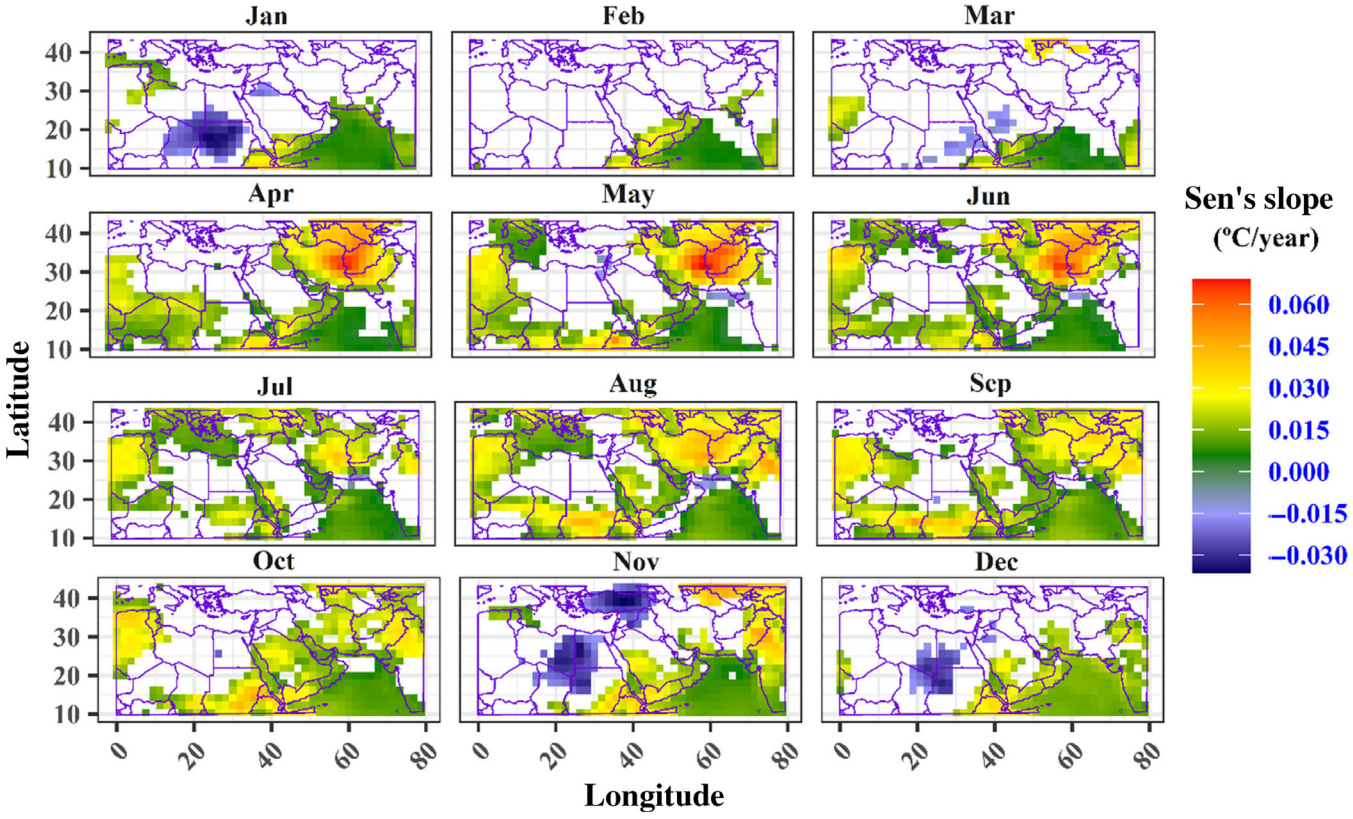

FIGURE 7 Similar to Figure 5, but for the period 1942–2012. [Colour figure can be viewed at wileyonlinelibrary.com]

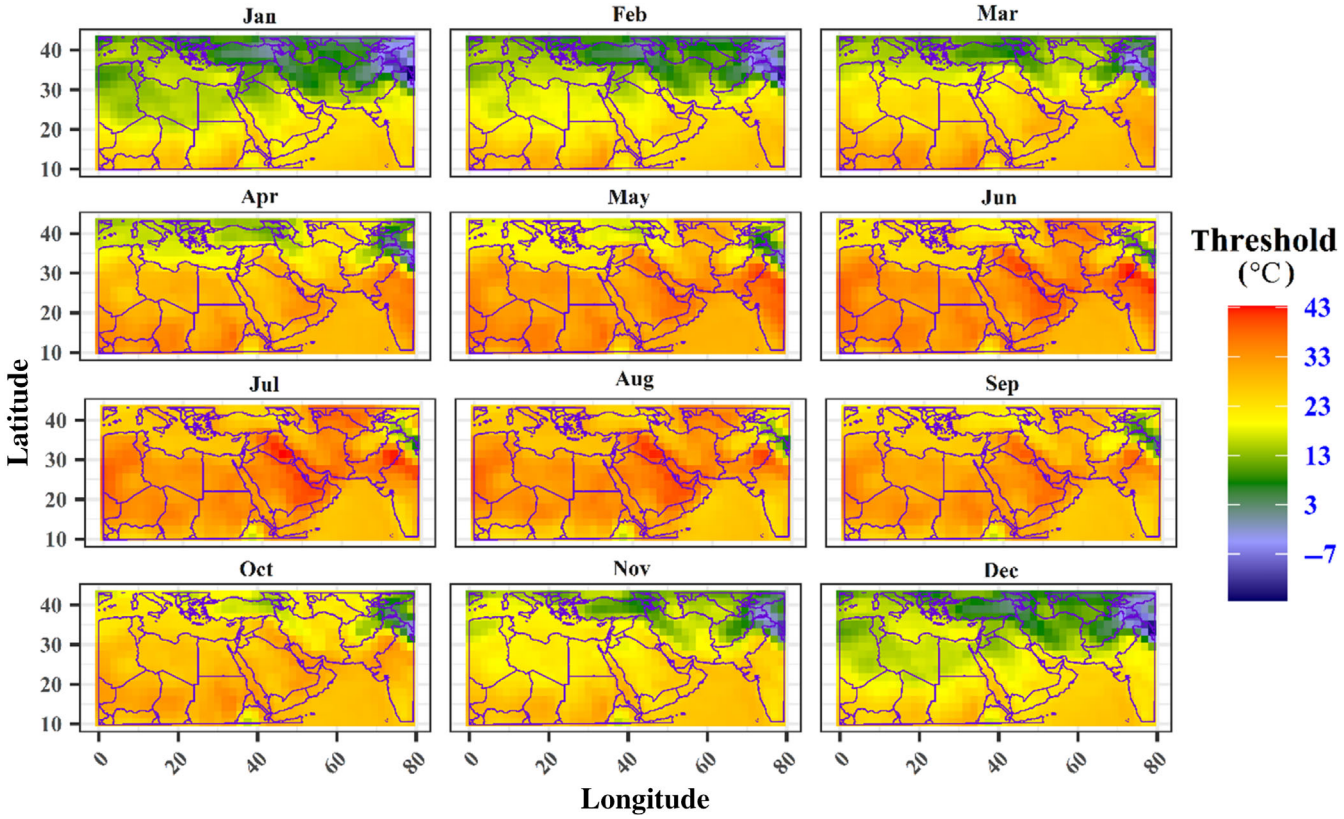

FIGURE 8 Temperature thresholds for determining heat days in the period from 1871 to 2012. [Colour figure can be viewed at wileyonlinelibrary.com]

As can be seen from Figure 8, the temperature threshold for determining heat days changes both temporally (in different months) and spatially. On average, across the study area, the highest heat days are observed in June (30.7) and July (31.1), and the lowest in the winter months of January (16.1) and December (17.3). The spatial coefficient variation of the thresholds shows that the winter months (especially January with 51%) have high values compared to the summer months (especially July with 16%). Due to the large extension of the studied area, in January at high latitudes even very negative values can be considered as a threshold for determining a heat day, while at lower latitudes this value is very high. The lowest threshold value (−4.16°C) is observed in January at the point 78.5° E and 33° N on the high Himalayan Mountain range due to the very cold climate that prevails throughout the year. That is, if the air temperature in this area is higher than −4.16°C in January, it can be called a heat day. On the other hand, the highest temperature threshold for a heat day is 43.2°C in July at a point at 45° E and 31.5° N, which includes a region in the southeast of Iraq.

Thresholds for two 71-year periods between 1871 to 1941 and 1942 to 2012 were also calculated, and here, for brevity, the difference between the second and first periods was calculated (Figure 9). On average, positive difference values were found in all months of the year. However, the amount of this difference is lower in March (0.06°C) and reaches its highest value in December (1.01°C). March has the highest spatial coefficient of variation, as both positive and negative values are close to each other. In terms of geographical location, the highest positive difference in the threshold can be seen in August by 4.4°C, at 76.9° E and 29.5° N in the south of the Himalayan Mountains. Thus, compared to the first period, the thresholds have increased significantly in the second period.

While the lowest negative difference observed in July at −2.11°C, at 37.5° E and 40.9° N in the south of the Black Sea in northern Turkey, which shows that in this region, the threshold value decreased significantly in the second period compared to the first period. The largest area with a positive difference can be seen in January with 98% area and then in December with 93%, and the lowest is 58% in March. However, in March more than half of the studied area has a higher temperature threshold in the second period than in the first period.

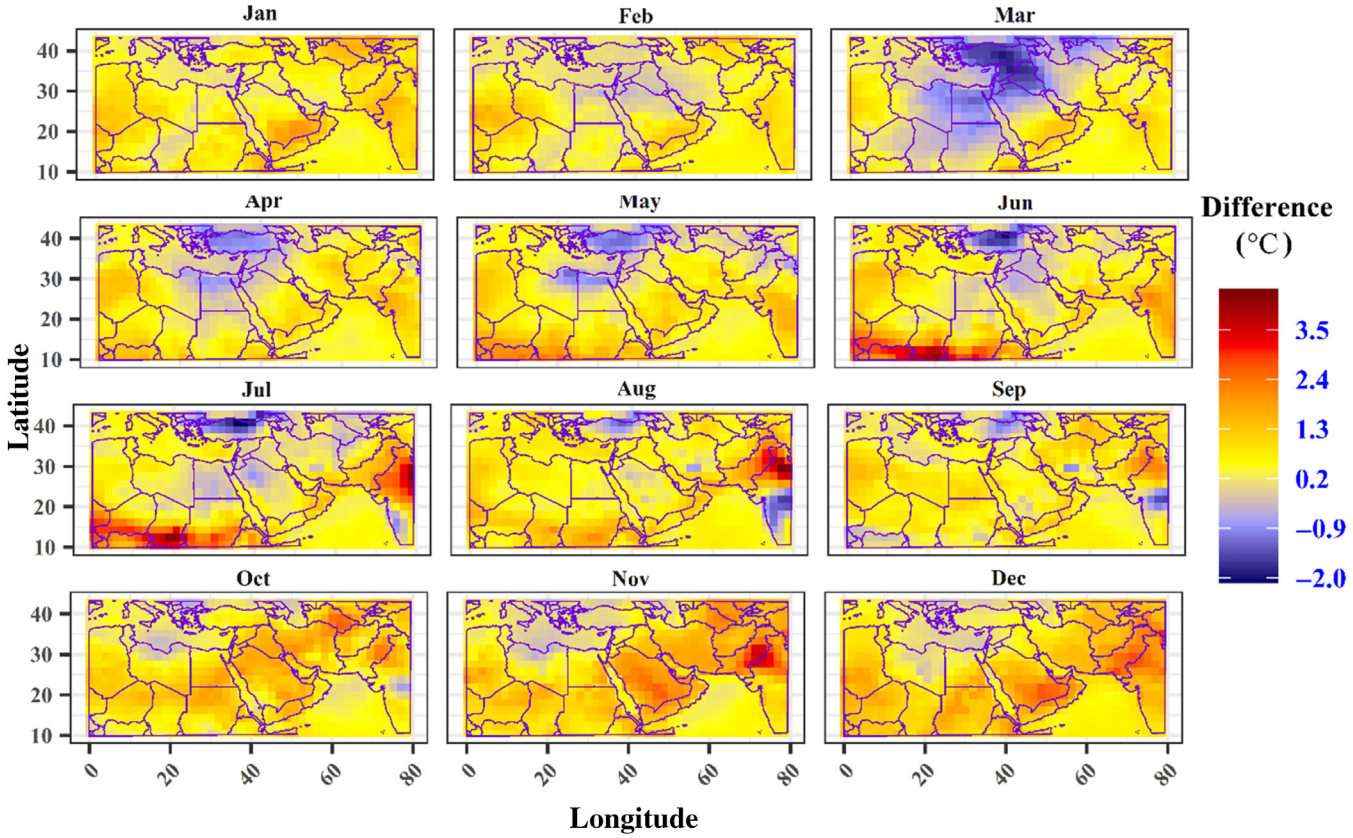

FIGURE 9 The difference between the thresholds for determining heat days in the period from 1871 to 1941 compared to the period from 1942 to 2012. [Colour figure can be viewed at wileyonlinelibrary.com]

3.3 | Some widespread heat days examples

Figure 10 shows the most widespread examples of heat days for each month. As can be seen in Figure 10, most of these examples occurred after 2000. Table 1 shows that the percentage of heat days is higher in the cold months than in the warm months. This is likely because in the summer, the temperature varies less and the region experiences uniformly warm temperatures. The most widespread heat day in the studied period is 1 November 2012, when 78% of the studied area was affected by a heat day with an average temperature of 23.1°C and a coefficient of variation of 26.6%. Although the 27 July 2011, heat day affected 35% of the area studied, it had the highest average temperature of 34.8°C and the lowest coefficient of variation of 11.1% during the study period.

3.4 | Decadal trend of WHDs

In this section, most WHDs for each decade were determined (for 14 decades) and then their trends were calculated. Based on the nonparametric Mann–Kendall test, a significant increase in WHDs can be found in May, August, October, November and December. According to Sen's slope statistics, the number of WHDs in the studied area increased by 2.4% per decade in November, which is more than compared to other months. The smallest increase occurred in March, where the number of heat days increased by 0.3%. In general, there was no decreasing trend in any of the months of the year, which shows that the heat days have continuously increased in the long term and have an upward trend.

The longest WHDs were calculated for each month of the year in two periods: 1871–1941 and 1942–2012, and then the monthly trends of these two periods were compared (Figure 11). In the first period, a statistically significant trend is observed only in January (increase) and April (decrease). Based on Sen's slope values, a decreasing trend is observed for WHDs in March, May, June, September and October. Thus, in contrast to the whole period (1871–2012), a decreasing trend is actually observed in WHDs in the region in the first study period. However, in the second period, the situation is different from the first period. There is an increasing trend in all months, which is quite significant in January, April, May, June, July, August, September and October according to the Mann–Kendall test. In the second study period, the highest rate of increase is in August, when WHDs increased by 0.37% (or 2.7 pixels) per year.

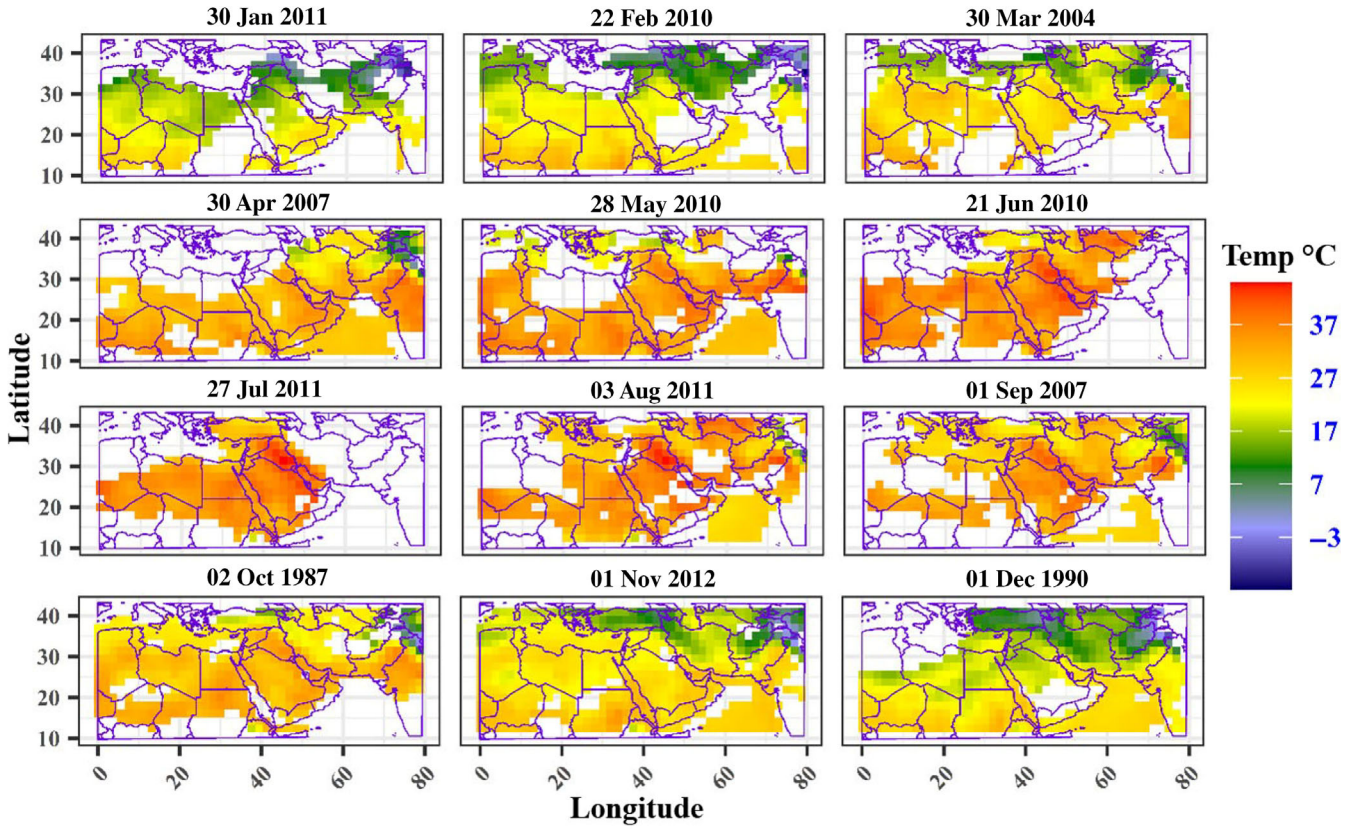

FIGURE 10 The most widespread heat days in the period from 1871 to 2012. [Colour figure can be viewed at wileyonlinelibrary.com]

Row	Date	Coverage %	Temperature (°C)	CV %
1	30 Jan 2011	46	18.2	38
2	22 Feb 2010	61	20.2	37
3	30 Mar 2004	56	23.6	25
4	30 Apr 2007	57	29.4	20.1
5	28 May 2008	56	31.8	16.7
6	21 Jun 2010	46	34.5	12.3
7	27 Jul 2011	35	34.8	11.1
8	03 Aug 2011	55	32.3	15.5
9	01 Sep 2007	54	30	18.8
10	02 Oct 1987	61	27.9	21.4
11	01 Nov 2012	78	23.1	26.6
12	01 Dec 1990	68	20.1	32.3

TABLE 1 Statistical characteristics of the most widespread days in the period from 1871 to 2012, separately for each month.

3.5 | Density of WHDs

Figure 12 shows the density of WHDs, indicating the frequency of their occurrence for each point. It should be noted that the maximum possible density for a pixel is 180 because only one WHD is selected for each month. In all months, at least 90% of the total area was affected by WHDs. However, this impact varied both temporally and spatially. As for the average density, the highest frequency of WHDs is observed in November, with an average of 43.3 ± 11.8 days, and in March, with an average of 40.1 ± 13.7 days. During the studied period, the summer months are generally less affected by WHDs. The lowest density is observed in July with an average of 21.1 ± 9.06 days and in June with an average of 22 ± 9.5 days. It is likely that this occurrence was caused by the lack of small temperature fluctuations in summer

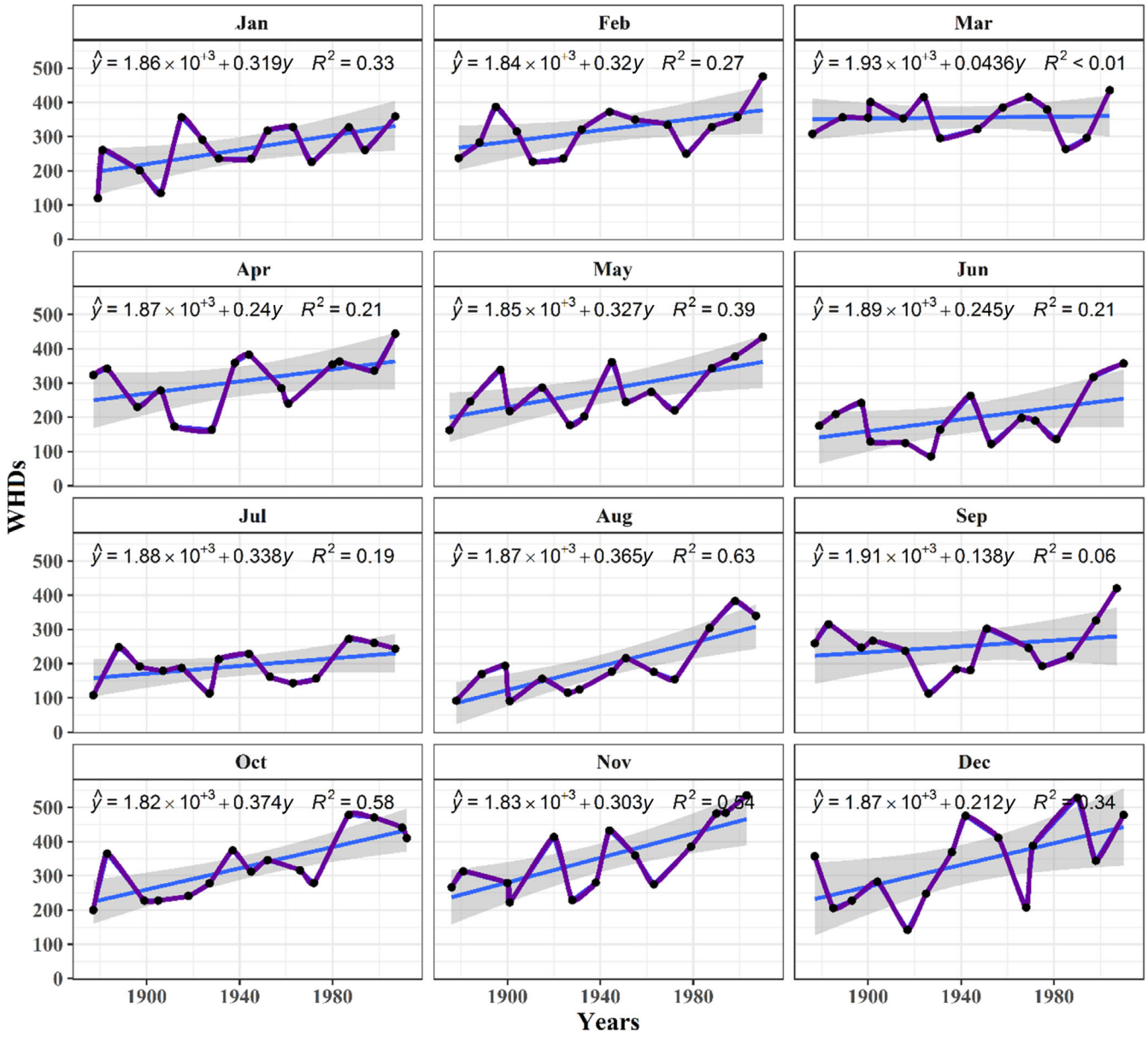

FIGURE 11 The decadal trend of widespread heat days (WHDs) in the period from 1871 to 2012. [Colour figure can be viewed at wileyonlinelibrary.com]

compared to the much higher fluctuations in winter, fall and spring. In other words, the temperature in the winter, autumn and spring months increased significantly during the period 1871–2012, which may lead to a shortening and shifting of the seasons in this region in the future. Spatially, the highest density of WHDs occurred with 71 recurrences in March at the point of 45° E and 33.3° N in eastern Iraq. This shows that this point was affected by WHDs in half of the year in March. While the lowest density of WHDs is also seen in the peripheral areas of the study area. The distribution of WHDs shows that the areas where the high frequency of heat days are located are mainly areas with a dry climate and poor vegetation covers such as deserts and very low altitudes, in the centre of the studied area, including parts of Iran, Iraq, Kuwait, Saudi Arabia, Egypt and Sudan. Due to their climatic nature in the subtropical desert belt, WHDs occur in these areas.

Figure 13 shows the difference in the WHDs density between two 71 years. The highest positive density difference, indicating a higher density of WHDs in the second period compared to the first period, is in November with an average of 11.8 ± 12 and in August with an average of 11.1 ± 10.7. In March, the difference in density is the smallest compared to the other months, which means that the WHDs decreases in the second period with an average of −0.18 ± 10.9. According to the results, the

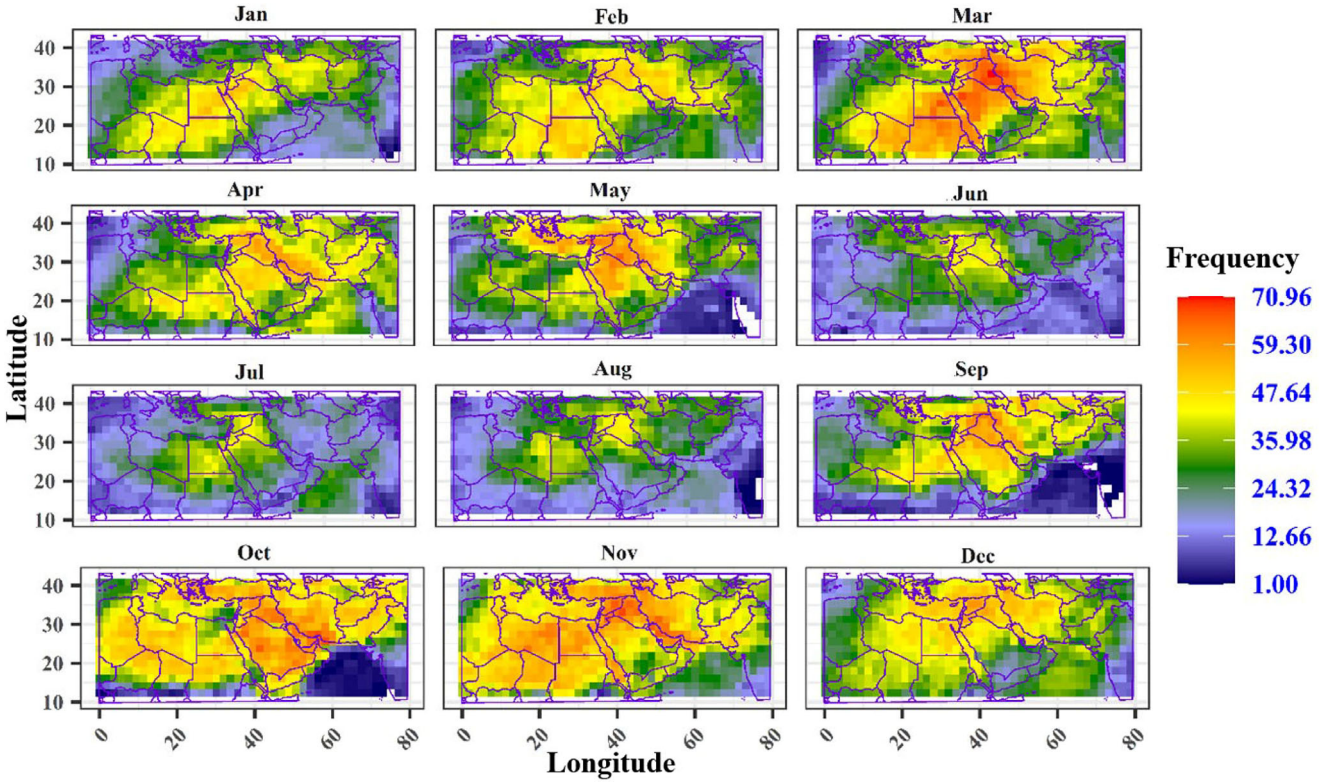

FIGURE 12 The density of widespread heat days in the period from 1871 to 2012. [Colour figure can be viewed at wileyonlinelibrary.com]

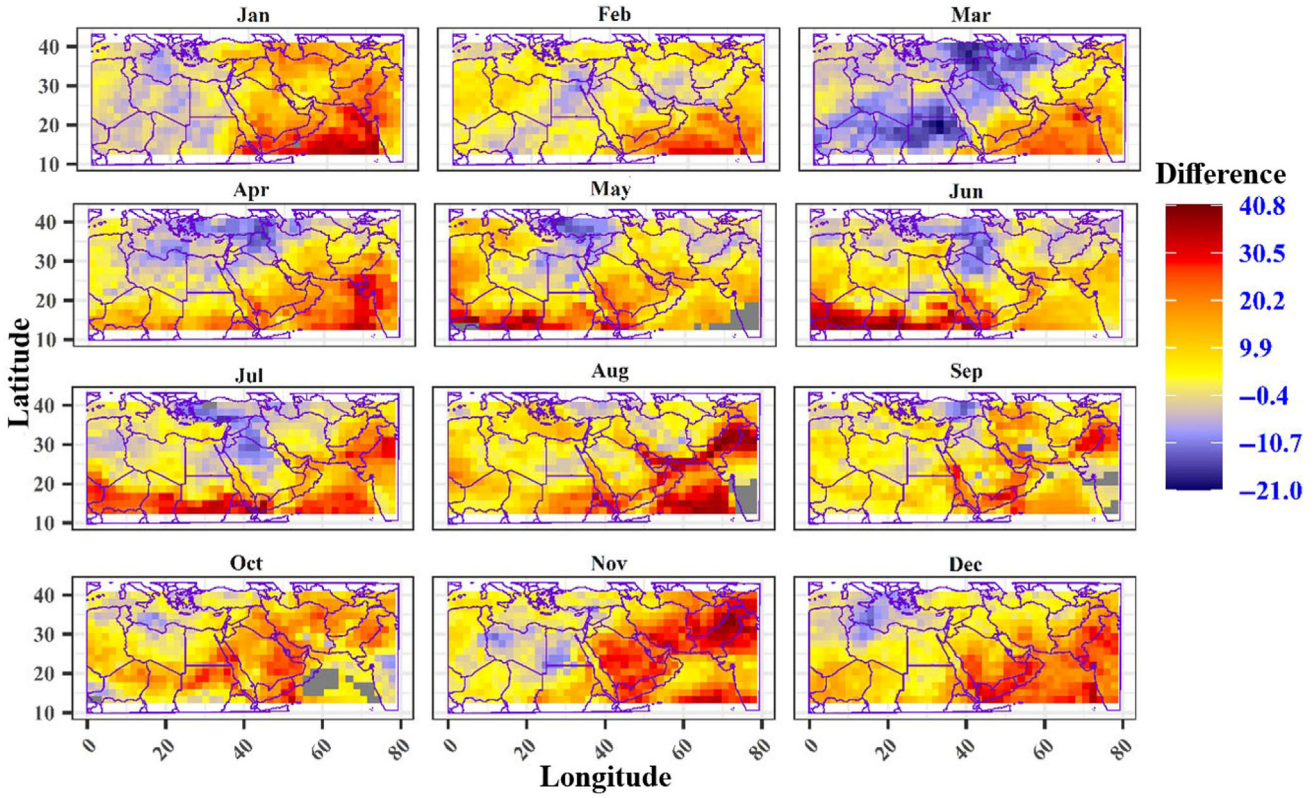

FIGURE 13 The difference in density of widespread heat days between the periods 1942 and 2012 compared to the period 1871 and 1941. [Colour figure can be viewed at wileyonlinelibrary.com]

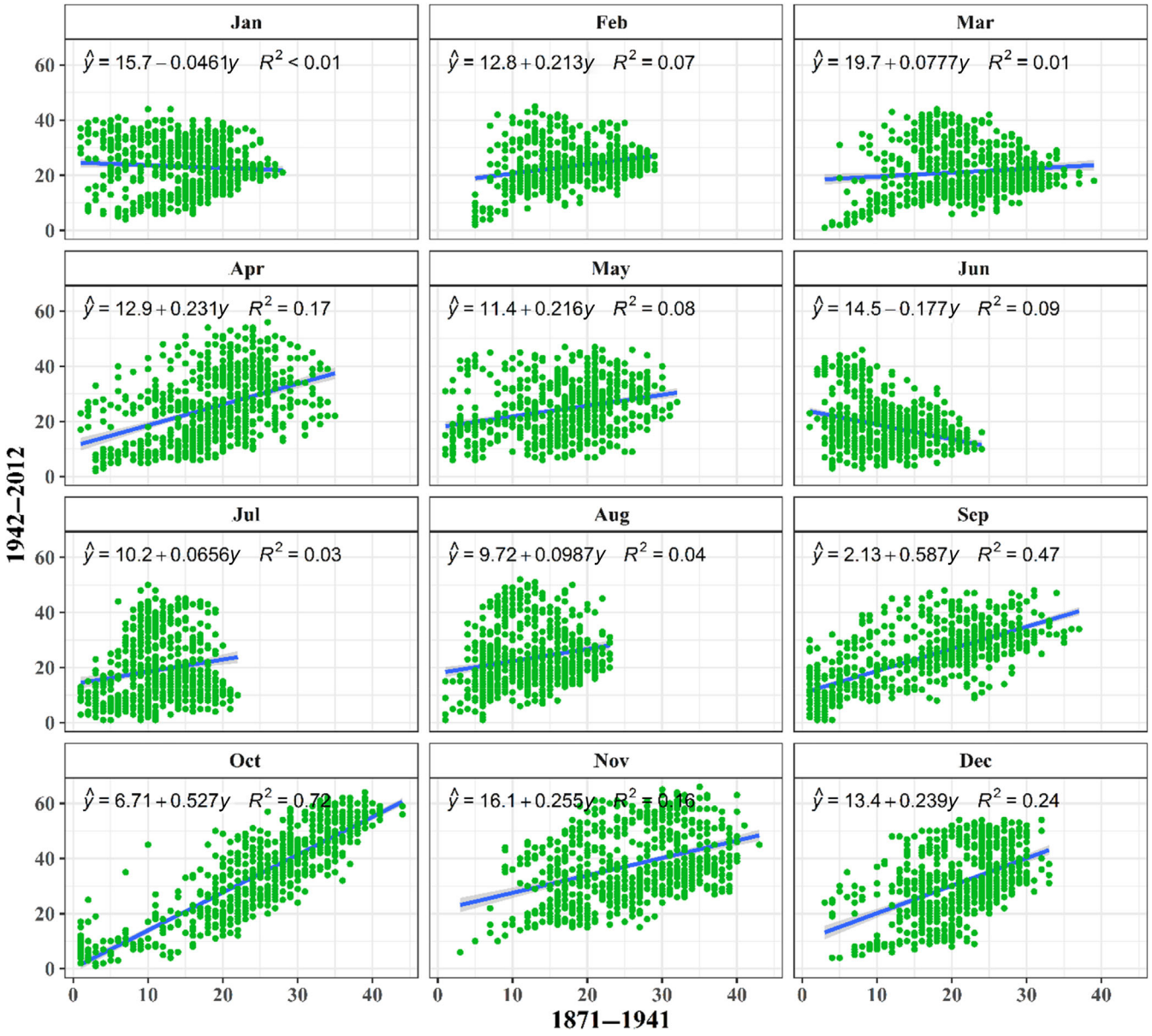

FIGURE 14 Spatial relationship of the occurrence of WHDs between 1942 and 2012 compared to 1871 to 1941. [Colour figure can be viewed at wileyonlinelibrary.com]

density of WHDs has increased in the second period (from 1942 to 2012). The main reason for this can be seen in global warming and the abnormal increase in ocean and land temperature after 1964 (Masson-Delmotte et al., 2018).

The density difference of the second period compared to the first period (Figure 13) is 40 samples at 72° E and 34.3° N in Pakistan near the Himalayan Mountains in November. While the largest amount of negative difference in density is −21, at the location of 32° E and 20.3° N, which is located in the north of Sudan.

Figure 14 spatially compares the WHDs density between the first and second periods. In general, the spatial relationship between the density of the first and second periods from January to August is not similar to each other. The coefficient of determination is very negligible in all months. In March of the second period, which has the lowest coefficient of determination, the concentration of WHDs is highest in northeast Africa, Egypt, Libya and northern Arabia, while in the first period, the highest occurrence of WHDs is observed in the countries of Sudan, Chad, Niger and eastern Iran. In the month of October, although the density of WHDs increased in the second period, the highest similarity between the two periods is observed with a coefficient of determination of 0.72%. Spatially, in this month, the highest density of WHDs in both periods is observed in northwestern Arabia and western Iraq.

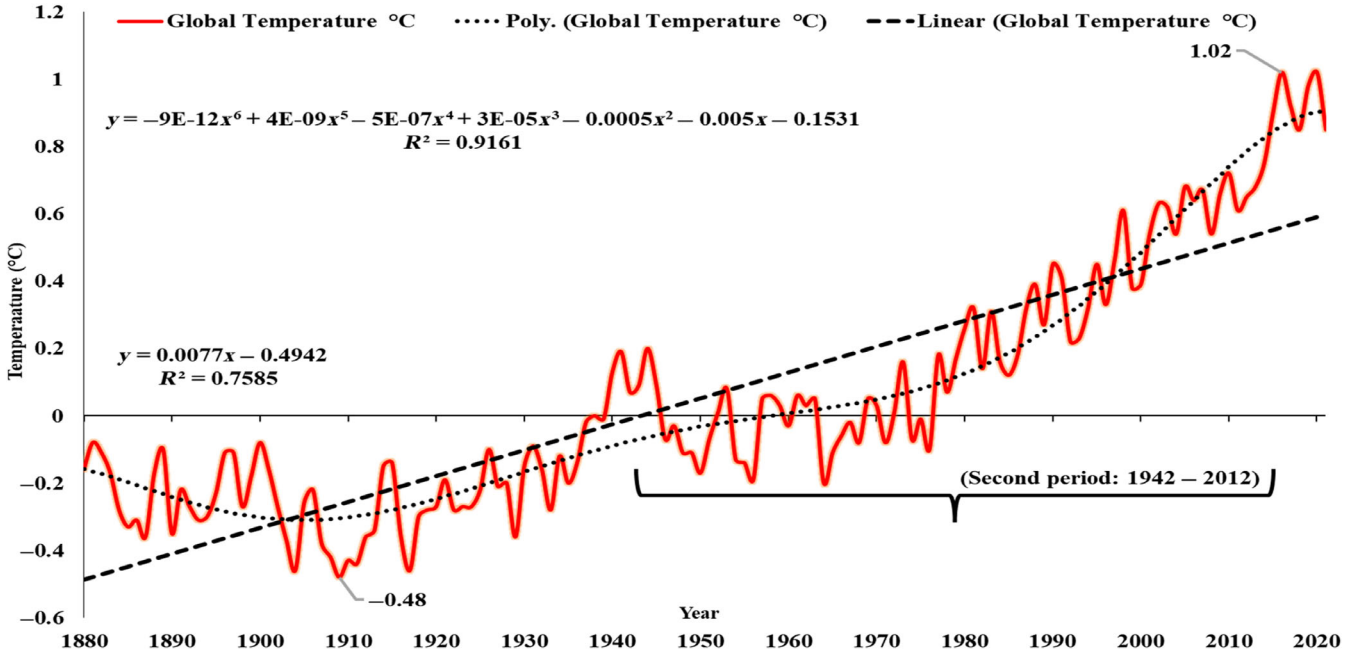

FIGURE 15 Anomalous time series of ocean and land temperatures index (global warming) in the period from 1880 to 2021 (*Data source*: https://data.giss.nasa.gov/gistemp). [Colour figure can be viewed at wileyonlinelibrary.com]

4 | DISCUSSION

Based on our findings, the occurrence of WHDs as an extreme climate event expanded from 1870 to 2015, with a predominant occurrence after 2000. Defining extreme events is often challenging due to the absence of a universally accepted definition of the term 'extreme,' as it is a relative concept (Stephenson et al., 2008). Certain studies have defined extreme events based on a probability distribution function that corresponds to the top 10% (or 1%) of extreme cases (Liberato et al., 2021; Tylkowski & Hojan, 2018), while others have identified extreme events using the *Z*-score index and anomaly values (Jones et al., 2021; Kubiak-Wójcicka et al., 2021). In the case of Liberato et al. (2021), the authors utilised the 10% probability distribution of extreme cases as a threshold to identify extreme events and subsequently calculated the percentage of pixels in the study area to determine the extent of the phenomenon. At the regional level, there are certain indicators that can aid in the examination of extreme events. The connected components labelling technique, which involves identifying regions in an image, proves valuable for segregating and enumerating objects (Falcao et al., 2004; Lee et al., 2007). Consequently, this method enables the identification of the most heavily impacted area by an extreme event and facilitates the assessment of its long-term trend. For example, Nikumbh et al. (2020) employed the connected component approach to identify extreme summer monsoon precipitation in India.

In this study, the WHDs index was utilised as a surrogate for temperature values to investigate the impact of global warming on the MENA region. The WHDs index represents the entirety of the MENA region, while temperature pertains to individual pixels. Although previous studies (Lelieveld et al., 2016; Zhang et al., 2005) have indicated an increase in temperatures in the MENA region, particularly during summer, the results obtained from the WHDs index may differ. While the spatial distribution of decreasing or increasing temperature trends (refer to Figure 5) can provide an overall perspective of the MENA, the outcomes derived from analysing regional temperature trends and WHDs exhibit disparities. For instance, the most prominent decreasing temperature trend (27% of the study area) was observed in Saudi Arabia, Iraq, western Iran, Syria and Turkey in March (as illustrated in Figure 5). However, there is no corresponding downward trend in WHDs for the same month. Consequently, it can be inferred that there is a lack of agreement between temperature and WHDs trends. When investigating the temperature trend in May, no significant trend is evident in many parts of the studied area. However, an analysis of WHDs trends reveals a substantial increasing trend over a 142-year period (refer to Figure 16). These findings align with previous research that suggests one of the consequences of climate change is the occurrence of extreme events (Luber & McGeehin, 2008; Stott, 2016), which is also observable in this study through the observed increase in the extent of WHDs.

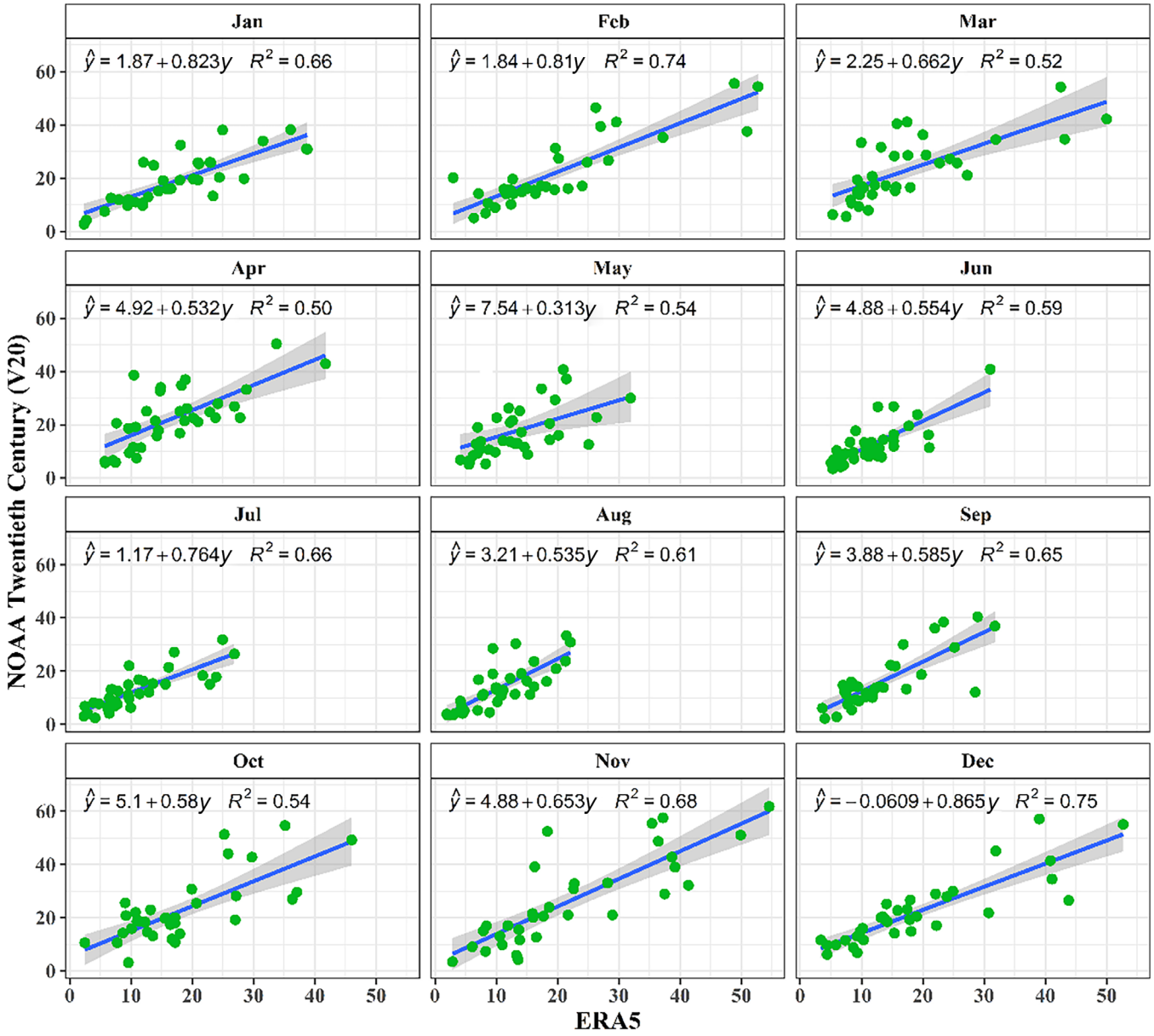

FIGURE 16 Monthly comparison of the percentage of area covered by widespread heat days between ERA5 and 20CRv2 data between 1979 and 2012. [Colour figure can be viewed at wileyonlinelibrary.com]

In addition to studying the long duration period of 142 years, all years were divided into two separate parts. For each time period, the threshold for determining WHDs was calculated independently. It is well-known that global warming has been influenced by human activities in recent years (Cook et al., 2016). Therefore, we aimed to investigate whether the increasing trend in temperature and WHDs could also be observed in the first period by eliminating the human effects that predominantly occurred after the 1990s (Epstein, 2000). Based on the findings of this study, there was no specific upward trend observed during the first period (1871–1941) when compared to the second period (1942–2012) (refer to Figures 6 and 7). As shown in Figure 15, the rate of global temperature increase was always negative from 1880 to 1937, reaching about 0.2°C for the first time in 1941. However, the increase in global temperature after 1964 was very rapid, and in 2016 it was more than 1°C. Therefore, the main reason for the increase in the number of WHDs in the second 71-year period with high probability is the increase in global temperature.

Larger datasets present enhanced opportunities for studying climate change and global warming. One of the strengths of this study is the utilisation of reanalysis data with a relatively long duration of 142 years, enabling the examination of WHDs trends over an extended period.

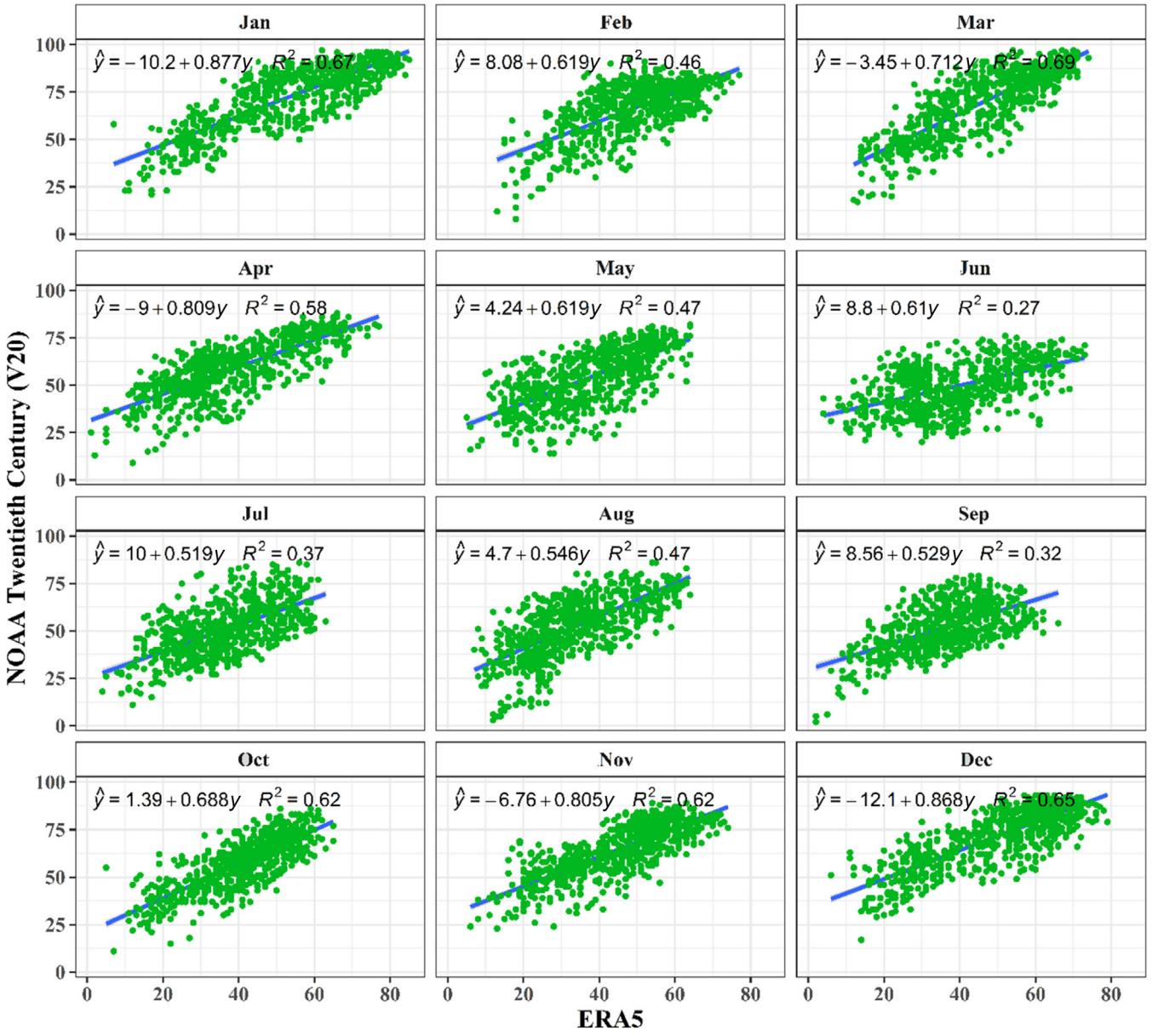

FIGURE 17 Spatial comparison of the percentage of area covered by widespread heat days between ERA5 and 20CRv2 data between 1979 and 2012. [Colour figure can be viewed at wileyonlinelibrary.com]

Gridded data were employed due to their continuous spatial coverage, making them highly suitable for calculating WHDs. Nevertheless, it is crucial to verify the validity of this data. To accomplish this, a comparison was conducted between the WHDs derived from 20CRv2 and the extent of heat days obtained from ERA5 reanalysed data. The relationship between the most WHDs based on the 20CRv2 reanalysis data and the ERA5 data was examined over a shared time span of 34 years, from 1979 to 2012. Initially, these two parameters were compared over time. Figure 11 illustrates the percentage of area covered by WHDs for the ERA5 and 20CRv2 pair. As depicted in the figure, the correlation coefficient exceeds 0.7 for all months of the year, with the highest correlation coefficient observed in December, reaching a coefficient of determination of 75%. This indicates that, overall, the temporal patterns of widespread heat day occurrences between these two databases are similar. Previous studies conducted in various regions worldwide have also demonstrated similar correlations between these data and ground-based synoptic stations, radiosondes, balloons, aircraft, as well as ERA-40, ERA-20c, ERA-Interim, ERA-5 and NNR data (Aalijahan et al., 2022; Bett et al., 2017; Brönnimann, 2017; Compo et al., 2011).

Furthermore, the spatial frequency of WHDs from the two databases was also compared (refer to Figure 17). Similar to the temporal comparison, a satisfactory relationship

between the frequency of WHDs in the ERA5 and 20CRv2 reanalysed data is evident in the spatial comparison. The highest correlation between these datasets is observed in March, with a coefficient of determination of 69%.

It is important to highlight that we selected one of the hottest regions in the world (Waha et al., 2017) for this study due to previous findings (Kumar et al., 2016) suggesting that arid areas are particularly susceptible to climate change. However, this study can be expanded to encompass a global scale, including higher latitudes, or explore other climatic variables such as precipitation.

5 | SUMMARY AND CONCLUSION

The objective of this study was to reconstruct the spatio-temporal accumulation of heat days in the MENA using the 20th century long-term reanalysis data from the NOAA organisation between 1871 and 2012. The following are the key conclusions drawn from our findings:

- The comparison of the heat days extracted from the 20th century data with the data from ERA5 showed that both data sets have a high correlation with each other.
- The long-term trend of temperature in the Middle East region was often a significant increase from August to February and a decrease from March to July. March, at 27%, and August, at 64%, occupy most of the regions with decreasing and increasing temperatures. In general, the increasing trend of temperature prevails over the decreasing trend in the MENA, and this increase was greater in the second study period (1942–2012) than in the first study period (1871–1941).
- Based on the 90% probability of occurrence, the temperature threshold for heat days was determined, which is different for each grid point due to its climate. This threshold was higher in the second period than in the first, indicating that the second period was warmer than the first period.
- The most widespread heat day of each month was determined based on the connected labels method. The most widespread days for each month occurred after 2000, and this trend was increasing, especially in the cold months. In general, the western parts of Iran, Syria, southern Turkey, Saudi Arabia, Kuwait, Egypt and northern Sudan had the highest density of WHDs in the region compared to other regions. In the second period, the extent of heat days increased compared to the first period, and the density of heat days increased in the second period compared to the first period.
- The spatial density correlation of the occurrence of WHDs between the first period and the second period showed that there is a negligible correlation between the two periods, indicating a change in the situation of WHDs in the second period compared to the first period.
- Overall, although temperature and the occurrence of WHDs (as extreme events) showed a long-term upward trend, these trends were not entirely consistent with each other. However, one of the main factors attributing to the significant increase in both temperature and WHDs during the second period is global warming. In the second period, global warming has taken a very strong upward trend, and as a result, the density of WHDS in the study area has increased significantly compared to the first period.

AUTHOR CONTRIBUTIONS

Mohammad Rezaei: Conceptualization; investigation; funding acquisition; writing – original draft; writing – review and editing; visualization; validation; methodology; software; formal analysis; project administration; resources; supervision; data curation. **Mehdi Aalijahan:** Investigation; funding acquisition; methodology; validation; visualization. **Anthony R. Lupo:** Writing – original draft; conceptualization. **Hadi Zerafati:** Validation; visualization; conceptualization; investigation.

DATA AVAILABILITY STATEMENT

The data that support the findings of this study are available from the corresponding author upon reasonable request.

ORCID

Mohammad Rezaei https://orcid.org/0000-0001-7380-4665

REFERENCES

Aalijahan, M., Karataş, A., Lupo, A.R., Efe, B. & Khosravichenar, A. (2023) Analyzing and modeling the spatial-temporal changes and the impact of GLOTI index on precipitation in the Marmara region of Türkiye. *Atmosphere*, 14(3), 489.

Aalijahan, M., Lupo, A.R., Salahi, B., Rahimi, Y.G. & Asl, M.F. (2022) The long-term (142 years) spatiotemporal reconstruction and synoptic analysis of extreme low temperatures (−15°C or lower) in the northwest region of Iran. *Theoretical and Applied Climatology*, 147(3), 1415–1436.

Aalijahan, M., Salahi, B. & Hatami, D. (2021) Investigating the relationship between changes in atmospheric greenhouse gases and discharge fluctuations in the basin of Aras River. *International Journal of Geography and Geography Education*, 44, 461–474.

Aalijahan, M., Salahi, B., Rahimi, Y.G. & Asl, M.F. (2019) A new approach in temporal-spatial reconstruction and synoptic analysis of cold waves in the northwest of Iran. *Theoretical and Applied Climatology*, 137(1), 341–352.

Ahmadalipour, A. & Moradkhani, H. (2018) Escalating heat-stress mortality risk due to global warming in the Middle East and North Africa (MENA). *Environment International*, 117, 215–225.

Ahn, K.H. & Merwade, V. (2014) Quantifying the relative impact of climate and human activities on streamflow. *Journal of Hydrology*, 515, 257–266.

Alahmad, B., Shakarchi, A.F., Khraishah, H., Alseaidan, M., Gasana, J., Al-Hemoud, A. et al. (2020) Extreme temperatures and mortality in Kuwait: who is vulnerable? *The Science of the Total Environment*, 732, 139289.

Al-Ghussain, L. (2019) Global warming: review on driving forces and mitigation. *Environmental Progress & Sustainable Energy*, 38(1), 13–21.

Almazroui, M., Islam, M.N., Dambul, R. & Jones, P.D. (2014) Trends of temperature extremes in Saudi Arabia. *International Journal of Climatology*, 34(3), 808–826.

Amrender, K., Singh, K.N., Chattopadhyay, C., Vennila, S. & Rao, V.U.M. (2015) Non-parametric analysis of long-term rainfall and temperature trends in India. *Journal of the Indian Society of Agricultural Statistics*, 69(2), 135–147.

Bett, P.E., Thornton, H.E. & Clark, R.T. (2017) Using the twentieth century reanalysis to assess climate variability for the European wind industry. *Theoretical and Applied Climatology*, 127(1), 61–80.

Bou-Zeid, E. & El-Fadel, M. (2002) Climate change and water resources in the Middle East: a vulnerability and adaptation assessment. *Journal of Water Resources Planning and Management*, 128, 343–355.

Brönnimann, S. (2017) Weather extremes in an ensemble of historical reanalyses. In: Brönnimann, S. (Ed.) *Historical weather extremes in reanalyses*. Bern: Geographica Bernensia G92, pp. 7–22. Available from: https://doi.org/10.4480/GB2017.G92.01

Campbell, S., Remenyi, T.A., White, C.J. & Johnston, F.H. (2018) Heatwave and health impact research: a global review. *Health & Place*, 53, 210–218.

Can, A. & Atimtay, A.T. (2002) Time series analysis of mean temperature data in Turkey. *Journal of Applied Time Series*, 4, 20–23.

Changnon, S.A., Kunkel, K.E. & Reinke, B.C. (1996). Impacts and responses to the 1995 heat wave: A call to action. *Bulletin of the American Meteorological Society*, 77(7), 1497–1506. https://doi.org/10.1175/1520-0477(1996)077<1497:iartth>2.0.co;2

Cheng, W.L., Saleem, A. & Sadr, R. (2017) Recent warming trend in the coastal region of Qatar. *Theoretical and Applied Climatology*, 128(1), 193–205.

Compo, G.P., Sardeshmukh, P.D., Whitaker, J.S., Brohan, P., Jones, P.D. & McColl, C. (2013) Independent confirmation of global land warming without the use of station temperatures. *Geophysical Research Letters*, 40(12), 3170–3174.

Compo, G.P., Whitaker, J.S., Sardeshmukh, P.D., Matsui, N., Allan, R.J., Yin, X. et al. (2011) The twentieth century reanalysis project. *Quarterly Journal of the Royal Meteorological Society*, 137(654), 1–28.

Cook, J., Oreskes, N., Doran, P.T., Anderegg, W.R., Verheggen, B., Maibach, E.W. et al. (2016) Consensus on consensus: a synthesis of consensus estimates on human-caused global warming. *Environmental Research Letters*, 11(4), 048002.

Csardi, M.G. (2013). Package 'igraph'. Last accessed, 3(09), 1–436.

Cueto, R.O.G., Martínez, A.T. & Ostos, E.J. (2010) Heat waves and heat days in an arid city in the northwest of Mexico: current trends and in climate change scenarios. *International Journal of Biometeorology*, 54, 335–345.

Ding, T., Qian, W. & Yan, Z. (2010) Changes in hot days and heat waves in China during 1961–2007. *International Journal of Climatology*, 30(10), 1452–1462.

Easterling, D.R., Evans, J.L., Groisman, P.Y., Karl, T.R., Kunkel, K.E. & Ambenje, P. (2000) Observed variability and trends in extreme climate events: a brief review. *Bulletin of the American Meteorological Society*, 81(3), 417–426.

El Kenawy, A.M., Lopez-Moreno, J.I., McCabe, M.F., Robaa, S.M., Dominguez-Castro, F., Pena-Gallardo, M. et al. (2019) Daily temperature extremes over Egypt: spatial patterns, temporal trends, and driving forces. *Atmospheric Research*, 226, 219–239.

Epstein, P.R. (2000) Is global warming harmful to health? *Scientific American*, 283(2), 50–57.

Esfandiari, N. & Rezaei, M. (2022) Automatic detection, classification, and long-term investigation of temporal–spatial changes of atmospheric rivers in the Middle East. *International Journal of Climatology*, 42(15), 7730–7750.

Falcao, A.X., Stolfi, J. & de Alencar, L.R. (2004) The image foresting transform: theory, algorithms, and applications. *IEEE Transactions on Pattern Analysis and Machine Intelligence*, 26(1), 19–29.

Fawzy, S., Osman, A., Doran, J. & Rooney, D.W. (2020) Strategies for mitigation of climate change: a review. *Environmental Chemistry Letters*, 18(6), 2069–2094.

Gherboudj, I., Beegum, S.N. & Ghedira, H. (2017) Identifying natural dust source regions over the middle-east and North-Africa: estimation of dust emission potential. *Earth-Science Reviews*, 165, 342–355.

Ghil, M. (2002) Natural climate variability. In: MacCracken, M. & Perry, J. (Eds.) *Encyclopedia of global environmental change*, Vol. 1. Chichester/New York: Wiley & Sons, pp. 544–549.

Hadi, S.J. & Tombul, M. (2018) Long-term spatiotemporal trend analysis of precipitation and temperature over Turkey. *Meteorological Applications*, 25(3), 445–455.

Hameed, M., Ahmadalipour, A. & Moradkhani, H. (2020) Drought and food security in the middle east: an analytical framework. *Agricultural and Forest Meteorology*, 281, 107816.

Hersbach, H., Bell, B., Berrisford, P., Hirahara, S., Horányi, A., Muñoz-Sabater, J. et al. (2020) The ERA5 global reanalysis. *Quarterly Journal of the Royal Meteorological Society*, 146(730), 1999–2049.

IPCC. (2023) Climate change 2023: synthesis report. In: Core Writing Team, Lee, H., & Romero, J. (Eds.) *Contribution of working groups I, II and III to the sixth assessment report of the Intergovernmental Panel on Climate Change*. Geneva, Switzerland: IPCC, pp. 35–115. https://doi.org/10.59327/IPCC/AR6-9789291691647

Masson-Delmotte, V., Zhai, P., Pörtner, H.O., Roberts, D., Skea, J., Shukla, P.R. et al. (Eds.). (2018) *Global warming of 1.5°C. An IPCC Special Report on the impacts of global warming of 1.5°C above pre-industrial levels and related global greenhouse gas emission pathways, in the context of strengthening the global response to the threat of climate change, sustainable development, and efforts to eradicate poverty*. Cambridge/New York: Cambridge University Press.

Jones, J.N., Boulton, S.J., Stokes, M., Bennett, G.L. & Whitworth, M.R. (2021) 30-Year record of Himalaya mass-wasting reveals landscape perturbations by extreme events. *Nature Communications*, 12(1), 6701.

Karl, T.R. & Easterling, D.R. (1999) Climate extremes: selected review and future research directions. *Climatic Change*, 42(1), 309–325.

Konisky, D.M., Hughes, L. & Kaylor, C.H. (2016) Extreme weather events and climate change concern. *Climatic Change*, 134(4), 533–547.

Koppe, C., Kovats, S., Jendritzky, G. & Menne, B. (2004) *Heat-waves: risks and responses (No. EUR/03/5036810)*. World Health Organization. Regional Office for Europe.

Kostopoulou, E., Giannakopoulos, C., Hatzaki, M., Karali, A., Hadjinicolaou, P., Lelieveld, J. et al. (2014) Spatio-temporal patterns of recent and future climate extremes in the eastern Mediterranean and Middle East region. *Natural Hazards and Earth System Sciences*, 14(6), 1565–1577.

Kousari, M.R., Ahani, H. & Hendi-zadeh, R. (2013) Temporal and spatial trend detection of maximum air temperature in Iran during 1960–2005. *Global and Planetary Change*, 111, 97–110.

Kubiak-Wójcicka, K., Nagy, P., Zeleňáková, M., Hlavatá, H. & Abd-Elhamid, H.F. (2021) Identification of extreme weather events using meteorological and hydrological indicators in the Laborec River catchment, Slovakia. *Water*, 13(10), 1413.

Kumar, S., Raizada, A., Biswas, H., Srinivas, S. & Mondal, B. (2016) Application of indicators for identifying climate change vulnerable areas in semi-arid regions of India. *Ecological Indicators*, 70, 507–517.

Kunkel, K.E., Pielke, R.A. & Changnon, S.A. (1999) Temporal fluctuations in weather and climate extremes that cause economic and human health impacts: a review. *Bulletin of the American Meteorological Society*, 80(6), 1077–1098.

Lee, D.R., Jin, S.H., Thien, P.C. & Jeon, J.W. (2007) FPGA based connected component labeling. In: *2007 International Conference on Control, Automation and Systems*. Seoul, Korea (South), IEEE, pp. 2313–2317.

Lehtonen, H. (1996) Potential effects of global warming on northern European freshwater fish and fisheries. *Fisheries Management and Ecology*, 3(1), 59–71.

Lelieveld, J., Proestos, Y., Hadjinicolaou, P., Tanarhte, M., Tyrlis, E. & Zittis, G. (2016) Strongly increasing heat extremes in the Middle East and North Africa (MENA) in the 21st century. *Climatic Change*, 137(1), 245–260.

Liang, L., Li, L. & Liu, Q. (2010) Temporal variation of reference evapotranspiration during 1961–2005 in the Taoer River basin of Northeast China. *Agricultural and Forest Meteorology*, 150(2), 298–306.

Liberato, M.L., Montero, I., Gouveia, C., Russo, A., Ramos, A.M. & Trigo, R.M. (2021) Rankings of extreme and widespread dry and wet events in the Iberian Peninsula between 1901 and 2016. *Earth System Dynamics*, 12(1), 197–210.

Lindsey, R. & Dahlman, L. (2020) *Climate change: global temperature*. Available at: http://www.climate.gov [Accessed on 22nd March 2021]

Luber, G. & McGeehin, M. (2008) Climate change and extreme heat events. *American Journal of Preventive Medicine*, 35(5), 429–435.

Marx, W., Haunschild, R. & Bornmann, L. (2021) Heat waves: a hot topic in climate change research. *Theoretical and Applied Climatology*, 146(1), 781–800.

McMichael, A.J., Woodruff, R.E. & Hales, S. (2006) Climate change and human health: present and future risks. *The Lancet*, 367(9513), 859–869.

Middleton, N.J. & Sternberg, T. (2013) Climate hazards in drylands: a review. *Earth-Science Reviews*, 126, 48–57.

Miller, N.L., Hayhoe, K., Jin, J. & Auffhammer, M. (2008) Climate, extreme heat, and electricity demand in California. *Journal of Applied Meteorology and Climatology*, 47(6), 1834–1844.

Mirhoseini, H., Gandomkar, A., Afrous, A. & Abbassi, A. (2021) Investigation of changes in temperature series in the eastern regions of Iran in order to study regional changes. *Quarterly of Geography & Regional Planning*, 11(42), 125–141.

Nikumbh, A.C., Chakraborty, A., Bhat, G.S. & Frierson, D.M. (2020) Large-scale extreme rainfall-producing synoptic systems of the Indian summer monsoon. *Geophysical Research Letters*, 47(11), e2020GL088403.

Pal, I. & Al-Tabbaa, A. (2010) Long-term changes and variability of monthly extreme temperatures in India. *Theoretical and Applied Climatology*, 100(1), 45–56.

Peale, S.J. (1966). Dust belt of the Earth. *Journal of Geophysical Research*, 71(3), 911–933. https://doi.org/10.1029/jz071i003p00911

Perkins-Kirkpatrick, S.E. & Lewis, S.C. (2020) Increasing trends in regional heatwaves. *Nature Communications*, 11(1), 1–8.

Peters, R.L. (1990) Effects of global warming on forests. *Forest Ecology and Management*, 35(1–2), 13–33.

Rezaei, M., Mielonen, T. & Farajzadeh, M. (2022) Climatology of atmospheric dust corridors in the Middle East based on satellite data. *Atmospheric Research*, 280, 106454.

Rezazadeh, M., Irannejad, P. & Shao, Y. (2013) Climatology of the Middle East dust events. *Aeolian Research*, 10, 103–109.

Robeson, S.M. (2004) Trends in time-varying percentiles of daily minimum and maximum temperature over North America. *Geophysical Research Letters*, 31(4), 1–4.

Robinet, C. & Roques, A. (2010) Direct impacts of recent climate warming on insect populations. *Integrative Zoology*, 5(2), 132–142.

Salman, S.A., Shahid, S., Ismail, T., Chung, E.S. & Al-Abadi, A.M. (2017) Long-term trends in daily temperature extremes in Iraq. *Atmospheric Research*, 198, 97–107.

Sen, P.K. (1968) Estimates of the regression coefficient based on Kendall's tau. *Journal of the American Statistical Association*, 63(324), 1379–1389.

Slivinski, L.C., Compo, G.P., Whitaker, J.S., Sardeshmukh, P.D., Giese, B.S., McColl, C. et al. (2019) Towards a more reliable historical reanalysis: improvements for version 3 of the twentieth century reanalysis system. *Quarterly Journal of the Royal Meteorological Society*, 145(724), 2876–2908.

Stephenson, D.B. (2008). Definition, diagnosis, and origin of extreme weather and climate events. *Climate Extremes and Society*, 11–23. https://doi.org/10.1017/cbo9780511535840.004

Stott, P. (2016) How climate change affects extreme weather events. *Science*, 352(6293), 1517–1518.

Thomas, N.P., Bosilovich, M.G., Marquardt Collow, A.B., Koster, R.D., Schubert, S.D., Dezfuli, A. et al. (2020) Mechanisms associated with daytime and nighttime heat waves over the contiguous United States. *Journal of Applied Meteorology and Climatology*, 59(11), 1865–1882.

Trenberth, K.E., Dai, A., Van Der Schrier, G., Jones, P.D., Barichivich, J., Briffa, K.R. et al. (2014) Global warming and changes in drought. *Nature Climate Change*, 4(1), 17–22.

Tylkowski, J. & Hojan, M. (2018) Threshold values of extreme hydrometeorological events on the polish Baltic coast. *Water*, 10(10), 1337.

Varotsos, C.A. & Efstathiou, M.N. (2019). Has global warming already arrived? *Journal of Atmospheric and Solar-Terrestrial Physics*, 182, 31–38. https://doi.org/10.1016/j.jastp.2018.10.020

Waha, K., Krummenauer, L., Adams, S., Aich, V., Baarsch, F., Coumou, D. et al. (2017) Climate change impacts in the Middle

East and northern Africa (MENA) region and their implications for vulnerable population groups. *Regional Environmental Change*, 17, 1623–1638.

Wang, X., He, K. & Dong, Z. (2019) Effects of climate change and human activities on runoff in the Beichuan River basin in the northeastern Tibetan plateau, China. *Catena*, 176, 81–93.

Yadollahie, M. (2019) The flood in Iran: a consequence of the global warming? *The International Journal of Occupational and Environmental Medicine*, 10(2), 54.

Yang, Y., Li, Q., Song, Z., Sun, W. & Dong, W. (2021) A comparison of global surface temperature variability, extremes and warming trend using reanalysis datasets and CMST-interim. *International Journal of Climatology*, 42(11), 5609–5628.

Zerafati, H., Ghavidel, Y. & Farajzadeh, M. (2021) Historical reconstruction and statistical survey on long-term temporal changes in temperatures above 50°C in West Asia. *Arabian Journal of Geosciences*, 14(21), 1–11.

Zhang, X., Aguilar, E., Sensoy, S., Melkonyan, H., Tagiyeva, U., Ahmed, N. et al. (2005) Trends in Middle East climate extreme indices from 1950 to 2003. *Journal of Geophysical Research Atmospheres*, 110(D22), 1–12.

Zheng, X., Streimikiene, D., Balezentis, T., Mardani, A., Cavallaro, F. & Liao, H. (2019) A review of greenhouse gas emission profiles, dynamics, and climate change mitigation efforts across the key climate change players. *Journal of Cleaner Production*, 234, 1113–1133.

Zittis, G., Hadjinicolaou, P., Fnais, M. & Lelieveld, J. (2016) Projected changes in heat wave characteristics in the eastern Mediterranean and the Middle East. *Regional Environmental Change*, 16(7), 1863–1876.

How to cite this article: Rezaei, M., Aalijahan, M., Lupo, A. R., & Zerafati, H. (2023). Trend analysis of widespread heat days in the Middle East and North Africa region between 1871 and 2012. *International Journal of Climatology*, 1–20. https://doi.org/10.1002/joc.8306